Identification of an N-terminal inhibitory extension as the primary mechanosensory regulator of twitchin kinase

Eleonore von Castelmur[a,1,2], Johan Strümpfer[b,c,1], Barbara Franke[a], Julijus Bogomolovas[a,d], Sonia Barbieri[a], Hiroshi Qadota[e], Petr V. Konarev[f], Dmitri I. Svergun[f], Siegfried Labeit[d], Guy M. Benian[e], Klaus Schulten[b,c], and Olga Mayans[a,3]

[a]Institute of Integrative Biology, University of Liverpool, Crown Street, Liverpool L69 7ZB, United Kingdom; [b]Center for Biophysics and Computational Biology, University of Illinois, Urbana, IL 61801; [c]Beckman Institute, University of Illinois, Urbana, IL 61801; [d]Department for Integrative Pathophysiology, Universitätsmedizin, 68167 Mannheim, Germany; [e]Department of Pathology, Emory University, Atlanta, GA 30322; and [f]European Molecular Biology Laboratory, Hamburg Outstation, c/o DESY, Notkestrasse 85, D-22603 Hamburg, Germany

Edited by* Angela M. Gronenborn, University of Pittsburgh School of Medicine, Pittsburgh, PA, and approved June 29, 2012 (received for review January 31, 2012)

Titin-like kinases are an important class of cytoskeletal kinases that intervene in the response of muscle to mechanical stimulation, being central to myofibril homeostasis and development. These kinases exist in autoinhibited states and, allegedly, become activated during muscle activity by the elastic unfolding of a C-terminal regulatory segment (CRD). However, this mechano-activation model remains controversial. Here we explore the structural, catalytic, and tensile properties of the multidomain kinase region of *Caenorhabditis elegans* twitchin (Fn^{31}-Nlinker-kinase-CRD-Ig^{26}) using X-ray crystallography, small angle X-ray scattering, molecular dynamics simulations, and catalytic assays. This work uncovers the existence of an inhibitory segment that flanks the kinase N-terminally (N-linker) and that acts synergistically with the canonical CRD tail to silence catalysis. The N-linker region has high mechanical lability and acts as the primary stretch-sensor in twitchin kinase, while the CRD is poorly responsive to pulling forces. This poor response suggests that the CRD is not a generic mechanosensor in this kinase family. Instead, the CRD is shown here to be permissive to catalysis and might protect the kinase active site against mechanical damage. Thus, we put forward a regulatory model where kinase inhibition results from the combined action of both N- and C-terminal tails, but only the N-terminal extension undergoes mechanical removal, thereby affording partial activation. Further, we compare invertebrate and vertebrate titin-like kinases and identify variations in the regulatory segments that suggest a mechanical speciation of these kinase classes.

molecular mechanobiology | phospho-transfer catalysis | steered molecular dynamics simulations

Mechanical signals generated during physical activity are critical to the development and regulation of muscle tissue, which undergoes constant adaptation to mechanical demand. Despite the physiological importance of this mechano-feedback, little is known about how mechanical signals are sensed by the myofibril and further translated into biochemical events that feed into the homeodynamics of the tissue. In this context, the giant proteins of the titin-like family (0.7–4 MDa) are emerging as key mechanotransducers in muscle. Proteins from this family include titin and obscurin in mammals; twitchin, the obscurin homolog UNC-89 and the small TTN-1 titin in nematodes and mollusks; projectin and stretchin in insects (1, 2). These proteins are composed of numerous Ig-like domains linked in series and form long filaments embedded in the sarcoskeleton. There, these proteins mediate passive mechanical processes that dictate myofibrillar elasticity and relaxation rates.

Titin-like proteins contain a conserved kinase region near their C terminus that consists of *Ig-Ig-Fn-linker-kinase-tail-Ig* domains. This conservation suggests that titin-like kinases are important members of signaling networks in the sarcomere, although little is known about their cellular context. Titin kinase (TK) and twitchin kinase (TwcK) are the best studied members of the family and have been linked to stretch-activated pathways in muscle (3, 4). In TK, the strain that develops in the cytoskeleton during muscle activity has been proposed to induce a conformational state that is recognized by the autophagosome receptors Nbr1 and p62 and the ubiquitin ligase MuRF2, which thereby are recruited to titin. These turn-over factors become released upon mechanical inactivity, going to repress the regenerative transcriptional response of the serum response factor (3). Further, the conserved *Ig-Ig-Fn* tandem preceding TK is a receptor site for the ubiquitin ligase MuRF1 (5, 6), which is linked to the atrophy that results from muscle disuse. In TwcK, mechanical stress has been correlated with increased kinase activity (4). These data suggest that titin-like kinases form mechanosensory signaling nodes central to myofibril regulation.

An insight into the regulatory mechanisms of these kinases came from the structural elucidation of TwcK from *C. elegans* (7, 8) and *Aplysia* (8) and human TK (9). The models agreed in revealing the kinase domain as autoinhibited by an approximately 50 amino acids (aa) long, C-terminal regulatory tail domain (CRD) that wedges itself between the two kinase lobes, blocking ATP binding. Catalytic activation appears to require CRD removal from the active site, but the mechanism of release remains controversial. Calmodulin has been shown to bind the CRD of TK and TwcK in vitro (10), but it does not lead to significant activation (9, 11). Recently, in agreement with the involvement of these kinases in stretch-mediated pathways, it has been suggested that the tension that builds up in the cytoskeleton during muscle function pulls the CRD from the kinase, causing its release by mechanical unfolding (3, 4). The stretch-activation of human TK studied by atomic force microscopy (AFM) and molecular dynamics (MD) simulations (12–15) indicated that strain might lead to an ordered sequence of conformational changes that unwind the CRD, leaving an active kinase core. Thus, these kinases could

Author contributions: E.v.C., J.S., B.F., J.B., S.B., H.Q., P.V.K., D.I.S., and O.M. designed research; E.v.C., J.S., B.F., J.B., S.B., H.Q., P.V.K., D.I.S., and O.M. performed research; G.M.B., S.L., and K.S. provided tools and materials; O.M. conceived the study; and J.S. and O.M. wrote the paper.

The authors declare no conflict of interest.

*This Direct Submission article had a prearranged editor.

Data deposition: The atomic coordinates and structure factors have been deposited in the Protein Data Bank, www.pdb.org (PDB ID code 3UTO).

[1]E.v.C. and J.S. contributed equally to this work.

[2]Present address: Netherlands Cancer Institute, Plesmanlaan 121, 1066 CX Amsterdam, The Netherlands.

[3]To whom correspondence should be addressed. E-mail: Olga.Mayans@liv.ac.uk.

This article contains supporting information online at www.pnas.org/lookup/suppl/doi:10.1073/pnas.1200697109/-/DCSupplemental.

act as stretch-sensors in the sarcomere mediating the translation of mechanical signals into signaling cascades.

Despite the apparent conservation of titin-like kinases, their mechanical, anatomical, and physiological contexts are highly diverse. It might be questioned whether all members of the family act as stretch-sensors and, if so, what are the speciation features that allow them to operate under their distinct mechanical regimes. To gain an insight into the molecular loading mechanism of these kinases, we have studied the structural, catalytic, and tensile properties of the *C. elegans* TcwK region. Our findings reveal new regulatory principles in this kinase family and shed light on the molecular basis of their individualized mechanical performances.

Results

Crystal Structure of the Multidomain Kinase Region from Twitchin. The crystal structure of the kinase region from *C. elegans* twitchin comprising the domains Fn^{31}-linker-kinase-CRD-Ig^{26} (TwcKR) has been elucidated to 2.4 Å resolution (Fig. 1 and Movie S1). The structure reveals the kinase in a tightly autoinhibited state, where both N- and C-terminal flanking segments occlude catalytic sites. The C-terminal fraction, CRD-Ig^{26}, wraps around the C-terminal kinase lobe as previously reported (8) (description and nomenclature in Fig. S1). The N-terminal region, consisting of domain Fn^{31} and the 47-aa long N-terminal linker (NL), wraps around the back of the N-terminal kinase lobe. Fn^{31} encloses the CRD, trapping it in its inhibitory position and restricting its external accessibility; while the NL segment consists of two distinct regions: (*i*) a tight "crown" that fits the groove between the N- and C-terminal kinase lobes and (*ii*) a frontal β-hairpin loop that docks into a crevice formed by the Fn^{31} and kinase domains. The contacts that Fn^{31} and NL make with the kinase-CRD fraction are described in Fig. 2, Fig. S2, and Table S1.

The NL crown has a prominent aromatic motif (129-YxxYx-FxxWxxYy-141) that mediates its packing against the kinase groove (Fig. 2*A*), resembling the regulatory C-terminal crown element of AGC kinases and the allosteric interaction of kinase Aurora-B with its activator (16). The NL motif of TwcKR is strongly conserved across twitchins and projectins of invertebrates (Fig. 2*C* and Fig. S3). In this motif, the N-terminal residue Y129 stacks against P447 of CRD-αR2 and binds to E160 from the N-terminal kinase lobe (Fig. 2*B*). Residues Y129 and E160 are strictly conserved across all kinases of this family and P447 is always a hydrophobic group, suggesting a high functional significance of these interactions. Notably, in TwcKR, this residue triad lies under the motif 124-TVSS-127 contributed by the NL itself, where T124, S126, and S127 are autophosphorylation sites (11). Based on their location at the kinase hinge region and at the edge of the ATP pocket, we expect that these conserved interactions might influence the transition between inactive and active catalytic states.

The β-hairpin at the NL front might also be of functional relevance. Here, residue R120 forms a salt bridge with E225 from the βC4-βC5 loop in the N-terminal kinase lobe, which, in turn, interacts with the catalytic helix H3 through an additional salt bridge, E221-R199 (Fig. 2*A*). Helix H3 (equivalent to helix αC of AGC kinases) hosts glutamate E201 that is central to ATP processing and strictly conserved across protein kinases (17). Thus, this set of interactions forms a relay system that links the NL β-hairpin to ATP catalytic groups. Notably, residue Y110 in the β-hairpin is lodged into a kinase pocket and is preceded by five positively charged residues in the sequence 104-RKRRRGY-110 (Fig. 2*B*). This sequence points to the possibility of Y110 being a phosphorylation site, with the positive residues coordinating the phosphate group. The βC4-βC5 loop is largely acidic (Fig. 2*C* and Fig. S3) and its negative charges might assist in inducing a conformational change in the NL β-hairpin upon phosphorylation. Tyrosine residues, segments rich in positively charged groups and a β-hairpin loop, are all conserved features of the NL regions of twitchins and projectins from invertebrates, but not mammalian titins (Fig. S3). The latter have a shorter NL segment (approximately 30 aa long) that is more distantly related in sequence and that lacks the frontal β-hairpin. In brief, the NL region appears to be an important mechanistic element in titin-like kinases, with its crown element predictably being generic across the family and the frontal β-hairpin conferring unique properties to invertebrate representatives.

Conformation of TwcKR in Solution. In the crystal structure, the packing of Fn^{31} against the kinase-CRD fraction involves few contacts and appears weak (Fig. S2 and Table S1). Thus, we explored whether the overall domain arrangement in the crystal is representative of TwcKR in solution using small-angle X-ray scattering (SAXS). The overall molecular parameters derived from scattering data, the experimental scattering pattern, and the pair distance distribution function $p(r)$ are given in Fig. 3. A comparison of the experimental radius of gyration R_g (33 ± 0.6 Å) with that calculated from the structure (28.7 Å) suggested that in solution TwcKR adopts a more extended conformation than in the crystal. Accordingly, the scattering pattern computed from the crystallographic model yielded a poor fit to SAXS data ($\chi = 3.31$), suggesting differences in the domain arrangement.

To estimate the differences between the crystalline and solution states, we interpreted the scattering data in terms of low-resolution models using ab initio (AB) shape determination and rigid body (RB) fitting of individual domain structures. In RB refinement, we first considered Fn^{31}, NL, kinase-CRD, and Ig^{26}

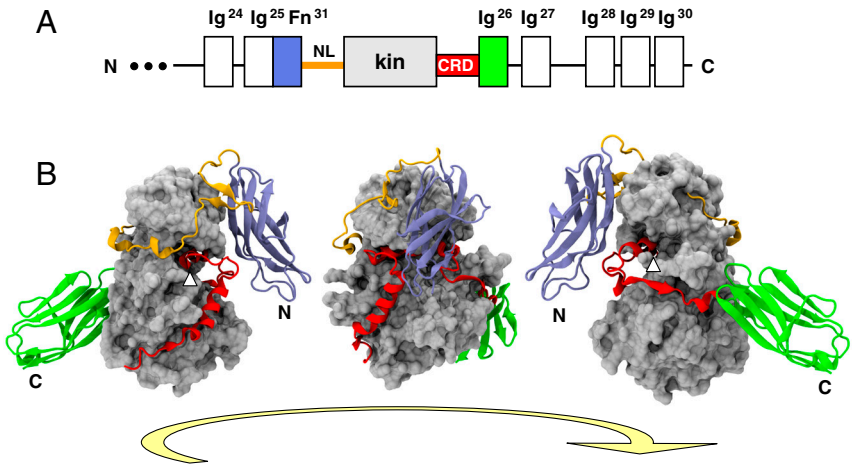

Fig. 1. Crystal structure of TwcKR (*A*) Domain composition of twitchin's C terminus. Domains studied in this work are colored; (*B*) Crystal structure in three rotating views. Helix αR2 that blocks the ATP binding site is indicated with a white pointer.

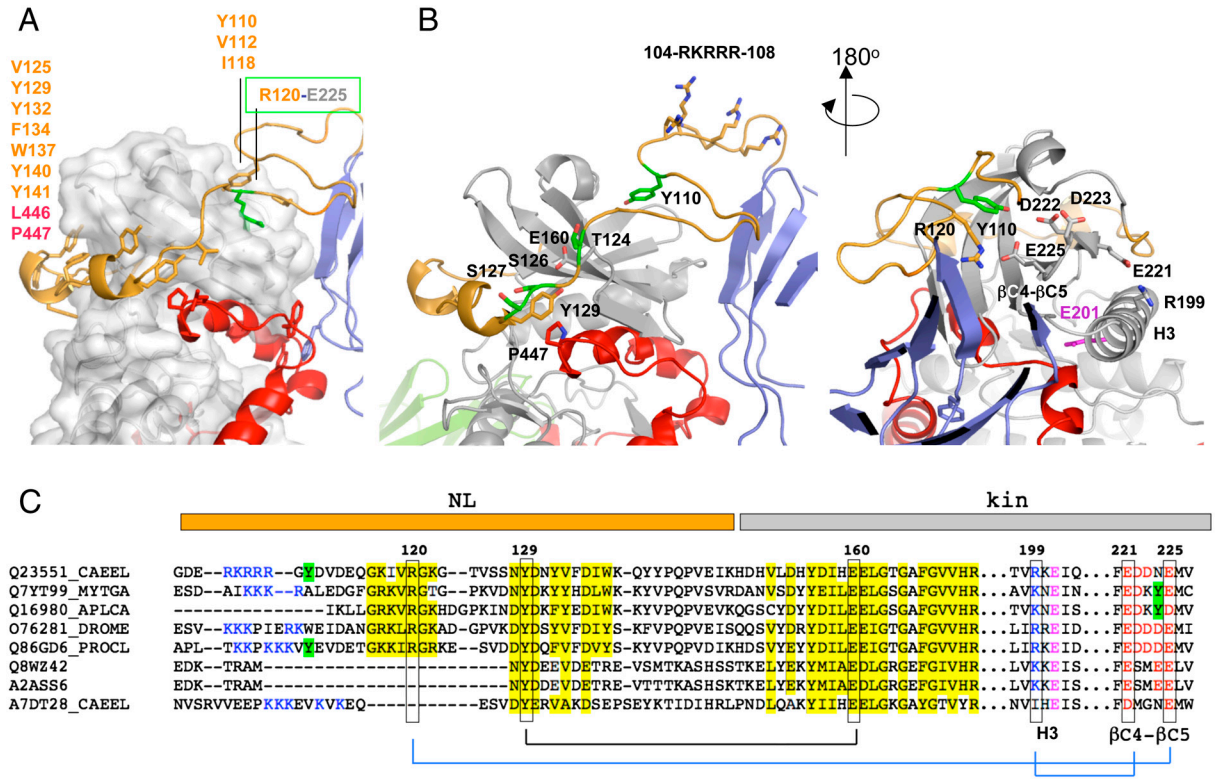

Fig. 2. The NL flanking region. (*A*) Hydrophobic groups mediating the packing of the NL against the kinase domain are listed. The buried salt bridge fixing the NL front to the kinase is highlighted; (*B*) Structural features of the NL segment in two views. Residues shown (or proposed to) undergo phosphorylation are in green. The strictly conserved tyrosine Y129 and its interacting residues are displayed. The cluster of positively charged residues (104–108) is shown. The catalytic glutamate in helix H3 is in magenta; (*C*) Motif conservation in the NL region. Sequences belong to TwcKs from *C. elegans* (Q23551), *Mytilus galloprovincialis* (Q7YT99), and *Aplysia californica* (Q16980); projectin from *Drosophila melanogaster* (O76281) and crayfish (Q86GD6); human (Q8WZ42) and mouse (A2ASS6) titin; and TTN-1 from *C. elegans* (A7DT28). Conservation is highlighted in yellow and interacting residues joined by lines. Positively charged residues at the NL front and negatively charged residues in the βC4-βC5 loop of the N-terminal kinase lobe are blue and red, respectively. Tyrosine residues in this region (or the structurally complementary region in mollusks) are marked in green. The similarity of twitchins and projectins, but not titins or TTN-1, is noticeable. A certain co-variation of the β-hairpin and the βC4-βC5 loop is detected. (Full sequence alignment of twitchins and projectins in Fig. S3).

as separate groups and allowed them to move independently. Once the similarity of the group arrangement to the crystal structure had been established (as in Fig. S4), we clustered them into multidomain rigid groups. The resulting SAXS models (Fig. 3*D*) agreed well and yielded good fits to the experimental data ($\chi_{AB} = 0.94$ and $\chi_{RB} = 1.04$, respectively). The models showed that the arrangement of the NL-kinase-CRD-Ig[26] fraction in the crystal structure agrees with that in solution. However, models had notable variations in the positioning of the Fn[31] domain. This variation suggested that in the sample population, on average, Fn[31] is not in direct contact with the CRD but in a more extended position in its vicinity. We interpreted this to signify that there is flexibility in the N-terminal region of the molecule, with Fn[31] alternating between a range of free and weakly interacting conformations. Based on the analysis of interactions held by residues of the NL segment (Table S1) and the atomic temperature factors of the crystallographic model in this region, we concluded that the flexibility is likely to originate from the positively charged motif 104-RKRRR-108 that links Fn[31] to the NL (Fig. 2*B*). In agreement with this view, this motif is disordered in one of the two copies of TwcKR in the crystallographic asymmetric unit.

We further analyzed flexibility in TwcKR using the ensemble optimization method (EOM) (18). For this analysis, we generated a pool of models where the Fn[31]-NL junction (sequence motif above) had been randomly generated to sample conformational variability (Fig. S5*A*). We then selected from this pool the models that best fitted the SAXS data (Fig. S5*B*). The obtained R_g distribution of the selected models (which are similar to RB models and provided fits with $\chi = 1.14$; Fig. 3*E*) shows a skewed peak around 3.2–3.3 nm confirming flexibility around Fn[31]. The R_g distribution is much narrower than that of the randomly generated pool, indicating that the structural flexibility is limited and that only relatively extended models similar to those computed (Fig. 3*D*) are present in solution. Thus, we conclude that the conformational variability in TwcKR primarily derives from the fluctuation of Fn[31].

Kinase Flanking Segments as Intrasteric Inhibitors. The CRD is a known intrasteric inhibitor in titin-like kinases, but the packing of the NL segment against the catalytic core suggests that this might also contribute to regulation. To test this hypothesis, we used [γ-[33]P]ATP to monitor catalytic phospho-transfer onto a model peptide substrate derived from MLCK (Fig. 4 and Fig. S6). The measurements were performed on TwcKR fragments corresponding to the isolated kinase domain (Kin), the kinase domain with either the NL (NL-Kin) or CRD (Kin-CRD) extension, the kinase domain flanked by both tails (NL-Kin-CRD), and the full-length TwcKR (Fig. 4*A*). Results showed that the isolated kinase domain has maximal activity, while the presence of either NL or CRD segments causes a moderate inhibition (Fig. 4 *B* and *C*). Both tails decreased activity comparatively (by approximately 40%), indicating that their regulatory significance is similar. Neither segment on its own can block catalysis, but their simultaneous presence in NL-Kin-CRD and TwcKR renders the kinase inactive (Fig. S6). These data suggests that the NL and CRD extensions act synergistically.

The finding that the CRD, which blocks the ATP binding site, permits high levels of residual catalysis is remarkable and unexpected. The finding points to a possible "looping out" mechanism of this tail when the NL is absent. The inhibition provided by the

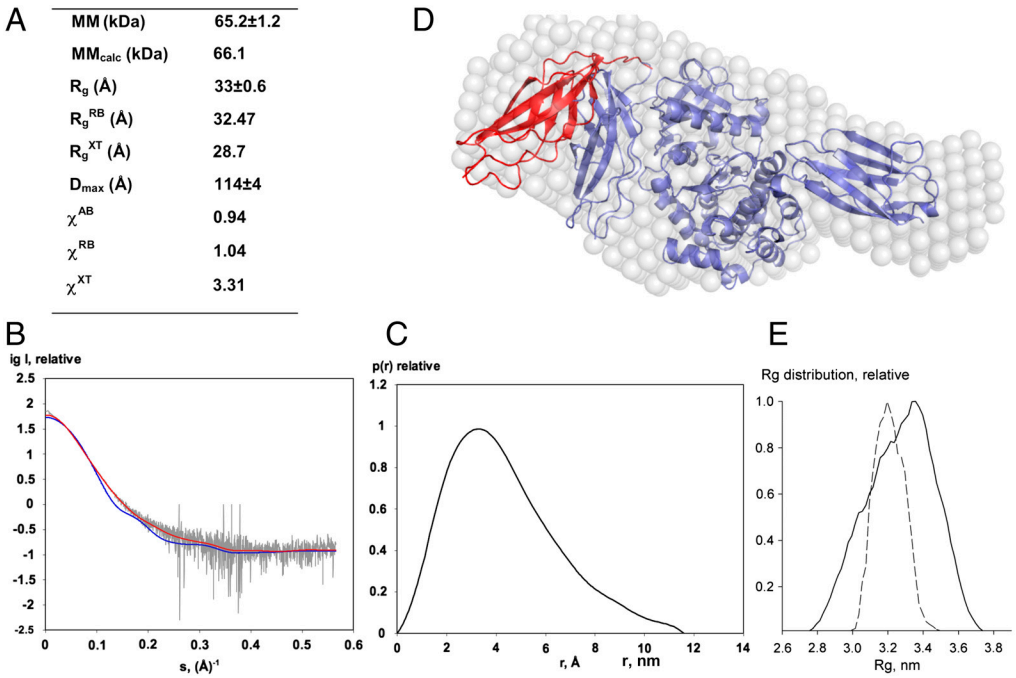

Fig. 3. SAXS analysis. (*A*) Molecular parameters calculated from SAXS data. MM, R_g, D_{max} denote the molecular mass, radius of gyration, and maximum size, respectively. Parameters without superscripts are experimental values; superscripts AB, RB, and XT refer to ab initio and rigid-body fitted models (shown in *D*) and the crystal structure, respectively. MMcalc is the theoretical MM computed from the protein sequence. χ is the discrepancy between experimental data and those computed from models; (*B*) SAXS data are displayed as dots with error bars (grey), while curves computed from the crystallographic (blue) and the RB model shown in (*D*) (red) are given as solid lines; (*C*) Distance distribution function; (*D*) Ab initio (white spheres) and RB (red) models are shown superimposed on the crystal structure (blue). In this RB model, only domain Fn^{31} was permitted to vary its position, while the rest of the molecule was fixed; (*E*) R_g distributions for models from a random pool of 10^5 structures (solid line) and optimized by EOM (dashed line).

NL segment agrees with deductions drawn from its structural features that suggest a role in restricting interlobular dynamics in the kinase. Abundant data on kinases such as IRTK (19), PKA, and PKC (20, 21) have shown that the opening-closure of the N-terminal kinase lobe underlies the transition between inactive and active states. We concluded that in TwcKR the NL might hinder the motions required for ATP catalysis.

Response of TwcKR to Directed Force Analyzed Through Simulation. To assess the response to stretch of NL and CRD inhibitory regions, we subjected the crystal structure to steered MD (SMD) simulations. First, TwcKR underwent free dynamics for 30 ns in an equilibrium simulation. The resulting conformation revealed that the structure remained stable overall (approximately 2.3 Å rmsd). However, an analysis of the equilibrated model showed that domain Fn^{31} had undergone a rocking motion and that the cluster of polar interactions that connected it to the kinase-CRD fraction had been disrupted (Fig. S7). This observation supports our previous deduction that these contacts are weak and that Fn^{31} is flexible.

SMD simulations were then performed on the equilibrated molecule, which was fixed at its N-terminal Cα atom while a force was applied to the C terminus at a stretching velocity of 5 Å/ns. The simulation continued until the first domain-unfolding event occurred, when the molecule had extended to 30% of its contour length, corresponding to 90 ns simulation time and 45 nm extension. The resulting force extension curve and its corresponding structural transitions are shown (Fig. 5 and Movie S2). Not surprisingly, the first event upon extension was the detachment of Fn^{31} from the CRD (force peak a1; FPa1). The ease of this removal was validated in independent simulations that applied constant low forces of 50 and 100 pN (over 70 ns simulation), where Fn^{31} release was the initial event (occurring in all cases within 50 ns simulation time). The second step was the unraveling of the NL and the C-terminal elements of the CRD (βR4 and αR3′) that occurred together and at low force. However, while the NL was fully released, the inhibitory CRD helices αR1 and αR2 remained firmly in place via interactions with the C-terminal kinase lobe. Further stretch caused unfolding of individual domains, with the N-terminal kinase lobe unfolding first (FPa5 and FPa6) followed by Fn^{31} (FPa7 and FPa8). The αR1-αR2 fraction of the CRD only unraveled after the N-terminal lobe had completely unfolded. Because such unfolded states are unlikely to represent physiological states, simulations were terminated here. To study whether the unfolding of NL and CRD in this simulation were influenced by the presence of the flanking domains Fn^{31} and Ig^{26}, which both interact weakly with the kinase, we analyzed separately the simulated stretch-response of the kinase core (including the CRD and the NL crown). The results were similar to those from simulations of the full-length TwcKR, as expected from the fact that Fn^{31} and Ig^{26} detach early in that simulation (Fig. S8 and Movie S3).

The stretch-response of *C. elegans* TwcKR has been previously measured by AFM (22). The agreement of our simulations with those data is excellent. Both AFM and MD show that the kinase domain unfolds before the flanking Fn^{31} and Ig^{26} domains and that kinase unfolding is a bilobal event, where the N-terminal lobe unfolds before the C-terminal one. AFM curves, however, did not identify force peaks that could be attributed to the unfolding of the CRD segment. The authors speculate that the CRD might have unfolded at very low force, undistinguishable from noise and below the interpretable events in AFM. Our data provide an alternative explanation by proposing that CRD unfolding does not occur as an independent event in those invertebrate kinases due to the tight binding of this extension to the C-terminal kinase lobe.

Here, we speculate that the readily accessible molecular state where NL and the C terminus of CRD (βR4 and αR3′) are unfolded, but all other elements remain structurally intact (including αR1 and αR2), might represent the mechanically primed state of TwcKR in its physiological context (a representative structure of this state can be seen approximately 25 s into Movie S3). However, it must be borne in mind that current computational simulations cannot reproduce physiological time scales and, thus, the

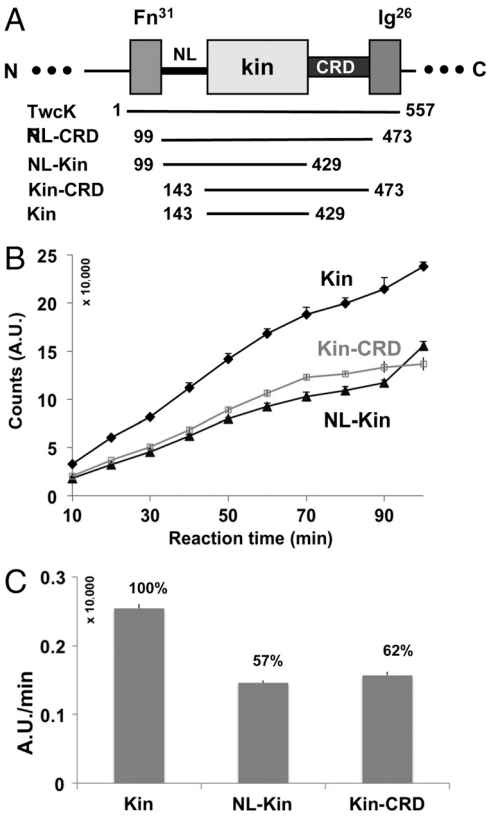

Fig. 4. TwcKR catalytic activity. (*A*) Domain boundaries of segments tested; (*B*) Diagram of catalytic traces and (*C*) relative enzymatic activities calculated by linear regression using points in the linear range (10–30 min; linear fit $R^2 > 90\%$). Full-length TwcKR and the NL-kinase-CRD construct were similarly inactive and their activity unquantifiable. Thus, they are not explicitly plotted here.

existence of alternative scenarios at physiological ranges remains a possibility. The CRD (in particular helices αR1 and αR2) is highly conserved across invertebrate twitchins and projectins (Fig. S3). Our calculations suggest that in these proteins the CRD behaves as an integral component of the lower kinase lobe and that the application of force, in the absence of other factors, is unlikely to cause its release from the catalytic core. The level of inhibition retained by the partly dislodged CRD is unknown, but catalytic data (Fig. 4) suggest that the removal of the NL in this mechanical state should result in partial, but notable, activation. Attaining full activity might follow yet unidentified mechanisms.

Discussion

Titin-like kinases are thought to act as mechanosensors in the sarcomere. These kinases exist in autoinhibited states and supposedly become activated by stretch-induced unfolding of their elastic, regulatory segments. Studies on TK (12–15) suggested the CRD as the main spring regulator in this kinase family, but results could not be reproduced for other members of the family (22). The current study, that considers TwcK within its neighboring protein context, has led us to identify an inhibitory segment that flanks the catalytic core N-terminally and that is the most mechanically labile region. The strict conservation of its 128-(N/D)YD-130…E-160 sequence motif across all members of the family (Fig. 2*B* and Fig. S3) and the fact that a pre-peak in AFM data of human TK (13) can now be interpreted as to indicate the early unfolding of this region also in that kinase, brings this segment forward as the primary mechanosensory regulator in this kinase family.

The results of the phosphorylation assay clearly show that both NL and CRD elements are jointly responsible for kinase inhibition. This, taken together with the fact that the NL is the first structural element to unfold and with the requirement that the CRD must be displaced for ATP to bind, provides strong support to the hypothesis that the N-linker hinders CRD removal. Notably, the CRD only affords moderate inhibition in TwcKR, revealing that its occupation of the ATP site is inefficient. We previously speculated that the CRD of titin-like kinases might "loop-out" upon binding of calmodulin (23). But it is conceivable that in the absence of the NL and when the amount of substrate is elevated, the kinase-αR2 interaction could be partly outcompeted. Such a mechanism would be relevant to mechanically primed states where the NL extension has been stretch-removed. In agreement with the permissive character of the CRD, stretch simulations on TwcKR only induced a modest rearrangement of this tail, being insufficient for its complete removal. It is possible that in TwcKR the CRD remains attached, to some extent, to the kinase throughout the catalytic cycle providing fold stability and protecting the active site from mechanical damage—resembling the mode of action of the C-terminal tail of VRK1 kinase (24). Mechanically primed states comprising a bound CRD must be catalytically active (equivalent to or higher than the Kin-CRD fragment assayed in this study; Fig. 4). However, stretch alone appears insufficient to induce full kinase activation. This finding suggests that additional, biochemical activation routes might exist in invertebrate muscle.

The results of this study on nematode TwcKR differ from previous simulations on human TK (12, 15), where a full unfolding of its CRD and the associated opening of the catalytic cleft occurred without compromising the integrity of the catalytic core. The velocity and geometry of our calculations on TwcKR were equiva-

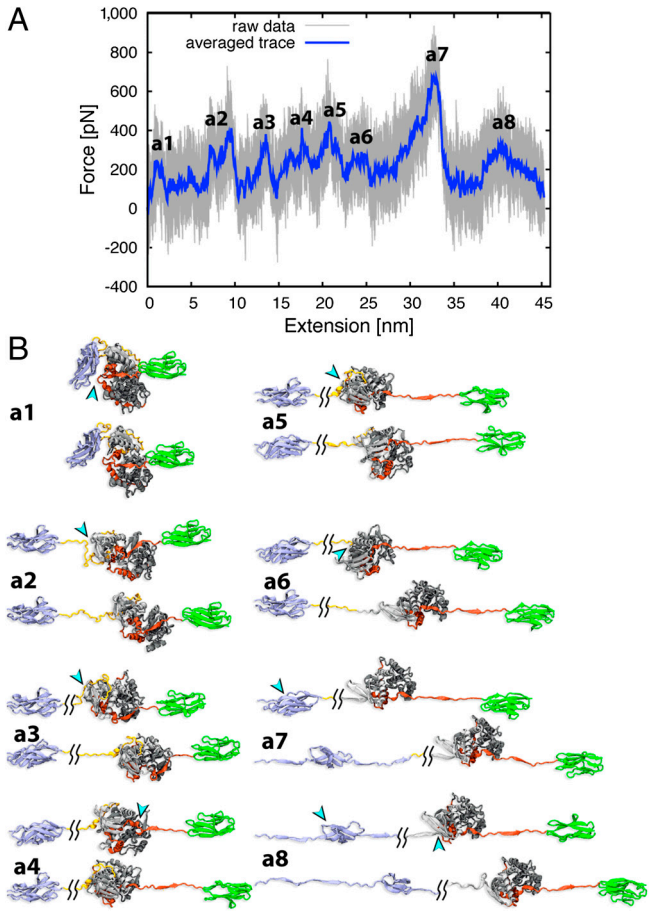

Fig. 5. MD simulations of TwcKR response to stretch. (*A*) Force extension curves and (*B*) stretch-induced conformational states corresponding to main mechanical events in simulations of TwcKR. The force peaks from primary unfolding events are labeled.

lent to those on TK. The contrasting outcome, however, correlates with actual differences in the composition, structure and interactions of the CRD in these kinases. The CRD of TK is shorter than that of TwcK by approximately 7 aas, it has a shorter αR1-αR2 connector, it lacks the secondary structure element helix αR3 (that is replaced by a loop), and the inhibitory helix αR2 is largely composed of small amino acids of the type Gly, Ala, and Ser (Figs. S3 and S9). As a consequence, the CRD in TK makes fewer interactions with the catalytic core than in TwcK (as confirmed by a comparison of the current crystal structure to entry 1TKI). Upon application of a pulling force, helix αR3 in TwcKR acts as a force-bearing barrier that preserves the CRD in its kinase-bound state. In TK, the substitution of this helix by a flexible loop suggests that, upon removal of strand β4, force immediately impinges on helix αR2 which, being composed of small residues, offers little resistance to unfolding. These molecular differences seem to reflect adaptations to specific mechanical contexts in the sarcomere. Thus, our findings question the stretch-sensor role of the canonical CRD tail as being generic across the kinase family.

The sensory regions of titin-like kinases from nematodes, insects, and mammals differ significantly. Nematodes and insects are important classes of invertebrate comprising parasitic worms, disease vectors, and crop pests that cause disease in human, animal, and plants. The TwcKRs of nematodes such as *Ascaris suum* that causes ascariasis, and *Brugia malayi* and *Loa Loa* that cause lymphatic filariasis share 70–75% sequence identity (seq.id.) with that of *C. elegans* in this study, while the projectin kinase region of insects share over 50% seq.id. (Fig. S3). Thus, twitchins and projectins predictably share the mechanistic principles described here, but diverge from the mammalian counterparts. It is yet to be investigated whether these differences might permit targeting these crucial kinases to combat infectious disease.

Methods

TwcKR (Q23551; residues 6108–6685; 6108 considered here as 1) and subfragments were expressed in *Escherichia coli* BL21(*DE3*) Rosetta2 (Novagen) and purified by affinity and size exclusion chromatography. Crystals grew from 20% PEG 600, 100 mM sodium citrate pH 5.5, 50 mM $MgCl_2$. Phasing was by molecular replacement. The two molecular copies in the asymmetric unit were virtually identical (0.56 Å rmsd for 556 Cα-atoms). Diffraction data and model are deposited with the Protein Data Bank (code 3UTO) and statistics are given in Table 1.

Table 1. X-ray data statistics and model refinement parameters

Diffraction data	
X-ray source	I02, Diamond (Didcot)
Detector	ADSC Quantum 315
Wavelength (Å)	0.9796
Spacegroup	$P2_12_12$
Unit cell	$a = 121.70$ Å, $b = 158.21$ Å, $c = 60.46$ Å
Molecules a.u./solvent content	2/44%
Resolution (Å)	19.8–2.4 (2.45–2.40)
Unique reflections	45313 (2670)
R_{sym} (I) (%)	9.7 (58.0)
I/σ (I)	14.43 (3.31)
Multiplicity	4.86 (4.82)
Completeness (%)	97.2 (96.9)
Model statistics	
R-factor/R_{free} (%)*	17.4/21.3
Nr protein residues/solvent atoms	1126/471†
rmsd bond/angle (°)	0.007/1.193

*The R-free set comprised 1165 reflections corresponding to 2.6% of the total data.

†Solvent atoms include those of the ordered buffer components hexaoxaicosane-diol, citrate, di(hydroxyethyl)ether, and glycerol.

Phosphorylation assays used 30 ng/mL kinase samples and 0.2 mg/mL of a peptide substrate (KKRARAATSNVFS) derived from kMLC11-23 (25). At time points, reaction mixture was withdrawn, spotted, and phosphoimaged.

SAXS data were collected from samples at 1.4, 2.5, 4.1 6.1 mg/mL. All data processing and molecular calculations used the ATSAS 2.4 suite of programs (EMBL, Hamburg).

All MD simulations were performed using NAMD 2.7 (26). Force-responses were probed by SMD simulations using the constant velocity stretching protocol (as in 27) with $\nu = 5$ Å/ns and a spring constant of $3k_BT/Å^2$.

(A comprehensive description of methods is given in *SI Text*).

ACKNOWLEDGMENTS. Supercomputer time was provided by the Texas Advanced Computing Center (MCA93S028 to J.S./K.S.). O.M. thanks the Diamond Light Source for synchrotron radiation time. We acknowledge the support of: the Royal Society (O.M.); Roche Research Foundation (O.M./E.v.C.); National Institutes of Health (NIH) (Grant R01-AR051466 to G.M.B.; Grants P41-RR005969 and R01-GM073655 to J.S./K.S.); and the American Heart Association (Grant 11GRNT7820000 to G.M.B.).

1. Bullard B, Linke WA, Leonard K (2002) Varieties of elastic protein in invertebrate muscles. *J Muscle Res Cell Motil* 23:435–447.
2. Kontrogianni-Konstantopoulos A, Ackermann MA, Bowman AL, Yap SV, Bloch RJ (2009) Muscle giants: Molecular scaffolds in sarcomerogenesis. *Physiol Rev* 89:1217–1267.
3. Lange S, et al. (2005) The kinase domain of titin controls muscle gene expression and protein turnover. *Science* 308:1599–1603.
4. Butler TM, Siegman MJ (2011) A force-activated kinase in a catch smooth muscle. *J Muscle Res Cell Motil* 31:349–358.
5. Centner T, et al. (2001) Identification of muscle specific ring finger proteins as potential regulators of the titin kinase domain. *J Mol Biol* 306:717–726.
6. Mrosek M, et al. (2007) Molecular determinants for the recruitment of the ubiquitin-ligase MuRF-1 onto M-line titin. *FASEB J* 21:1383–1392.
7. Hu SH, et al. (1994) Insights into autoregulation from the crystal structure of twitchin kinase. *Nature* 369:581–584.
8. Kobe B, et al. (1996) Giant protein kinases: Domain interactions and structural basis of autoregulation. *EMBO J* 15:6810–6821.
9. Mayans O, et al. (1998) Structural basis for activation of the titin kinase domain during myofibrillogenesis. *Nature* 395:863–869.
10. Gautel M, Castiglione-Morelli MA, Pfuhl M, Motta A, Pastore A (1995) A calmodulin-binding sequence in the C-terminus of human cardiac titin kinase. *Eur J Biochem* 230:752–759.
11. Lei J, Tang X, Chambers TC, Pohl J, Benian GM (1994) Protein kinase domain of twitchin has protein kinase activity and an autoinhibitory region. *J Biol Chem* 269:21078–21085.
12. Gräter F, Shen J, Jiang H, Gautel M, Grubmüller H (2005) Mechanically induced titin kinase activation studied by force-probe molecular dynamics simulations. *Biophys J* 88:790–804.
13. Puchner EM, et al. (2008) Mechanoenzymatics of titin kinase. *Proc Natl Acad Sci USA* 105:13385–13390.
14. Puchner EM, Gaub HE (2010) Exploring the conformation-regulated function of titin kinase by mechanical pump and probe experiments with single molecules. *Angew Chem Int Ed Engl* 49:1147–1150.
15. Stahl SW, Puchner EM, Alexandrovich A, Gautel M, Gaub HE (2011) A conditional gating mechanism assures the integrity of the molecular force-sensor titin kinase. *Biophys J* 101:1978–1986.
16. Gold MG, Barford D, Komander D (2006) Lining the pockets of kinases and phosphatases. *Curr Opin Struct Biol* 16:693–701.
17. Taylor SS, Kornev AP (2011) Protein kinases: Evolution of dynamic regulatory proteins. *Trends Biochem Sci* 36:65–77.
18. Bernadó P, Mylonas E, Petoukhov MV, Blackledge M, Svergun DI (2007) Structural characterization of flexible proteins using small-angle X-ray scattering. *J Am Chem Soc* 129:5656–5664.
19. Hubbard SR (1997) Crystal structure of the activated insulin receptor tyrosine kinase in complex with peptide substrate and ATP analog. *EMBO J* 16:5572–5581.
20. Johnson DA, Akamine P, Radzio-Andzelm E, Madhusudan M, Taylor SS (2001) Dynamics of cAMP-dependent protein kinase. *Chem Rev* 101:2243–2270.
21. Mastersona LR, et al. (2011) Dynamically committed, uncommitted, and quenched states encoded in protein kinase A revealed by NMR spectroscopy. *Proc Natl Acad Sci USA* 108:6969–6974.
22. Greene DN, et al. (2008) Single-molecule force spectroscopy reveals a stepwise unfolding of *Caenorhabditis elegans* giant protein kinase domains. *Biophys J* 95:1360–1370.
23. Wilmanns M, Gautel M, Mayans O (2000) Activation of calcium/calmodulin regulated kinases. *Cell Mol Biol (Noisy-le-grand)* 46:883–894.
24. Shin J, et al. (2011) NMR solution structure of human vaccinia-related kinase 1 (VRK1) reveals the C-terminal tail essential for its structural stability and autocatalytic activity. *J Biol Chem* 286:22131–22138.
25. Heierhorst J, et al. (1996) Substrate specificity and inhibitor sensitivity of Ca2+/S100-dependent twitchin kinases. *Eur J Biochem* 242:454–459.
26. Phillips JC, et al. (2005) Scalable molecular dynamics with NAMD. *J Comput Chem* 26:1781–802.
27. Lee EH, Hsin J, von Castelmur E, Mayans O, Schulten K (2010) Tertiary and secondary structure elasticity of a six-Ig titin chain. *Biophys J* 98:1085–1095.